RSC Advances

PAPER

View Article Online
View Journal | View Issue

Cite this: *RSC Adv.*, 2025, **15**, 16607

Fabrication of aramid-based antimicrobial polypropylene composite membranes functionalized with thiazolidine-based nanoparticles

Javaria Kanwal,[a] Sara Musaddiq, *[a] Sadia Iqbal,[a] Faryal Nazar Balouch,[a] Sajjad Ahmad,[b] Mohammad Abul Farah,[c] Mohammad Ajmal Ali[d] and Francis Verpoort [ef]

A series of 2-substituted 1,3-thiazolidine-4-carboxylic acid nanoparticle (TNP)-loaded aramid-based composite polypropylene (PP) membranes (**PM-1** to **PM-5**) have been fabricated *via* the phase-inversion method. For this purpose, the TNPs (**1a–5a**) were first synthesized by an anti-precipitation technique and characterized using ultraviolet-visible (UV/Visible) and X-ray diffraction (XRD) analyses. PP membranes loaded with TNPs were then prepared and characterized using scanning electron microscopy (SEM) and Fourier transform infrared (FTIR) analyses. The TNPs, and PP membranes loaded with the same, were subjected to antimicrobial evaluation against the Gram-negative bacteria *Escherichia coli* (*E. coli*). The TNPs exhibited significant antibacterial potential against the selected bacterial strains. Sample **3a**, *i.e.*, a nitro-substituted derivative of TNPs, was found to be the most active sample tested, with a 12 mm zone of inhibition. Similarly, all the PP membranes exhibited encouraging antifouling properties. Among them, membranes **PM-3** and **PM-5** loaded with nitro- and thienyl-substituted derivatives of TNPs (*i.e.*, **3a** and **5a**) exhibited excellent antifouling activity. In addition, the TNPs and loaded PP membranes were also screened for their antiviral potential against the Hemagglutinin 9 Neuraminidase 2 (H9N2) and Infectious Bronchitis Virus (IBV) viral strains, and TNPs **3a** and **5a** were found to be the most active antiviral agents, while the membranes loaded with the same, *i.e.*, **PM-3** and **PM-5**, also exhibited significant antiviral potential. This study presents the design and development of innovative composite membranes that can be used to efficiently disinfect water through the integration of advanced nanomaterials and refined fabrication techniques.

Received 1st February 2025
Accepted 29th April 2025

DOI: 10.1039/d5ra00748h

rsc.li/rsc-advances

1 Introduction

Access to fresh water is a critical need for human beings. However, clean water resources have been severely depleted in many places globally, causing difficulties and risking the lives of many. Multiple organic and inorganic contaminants pollute water and some of them are extremely persistent, unsafe and cancer-causing agents. Therefore, access to sufficient clean water resources has become a major challenge globally.

To address the growing scarcity of safe drinking water, it is crucial to prioritize water purification at the local level.[1] Traditional methods of purifying water, such as sedimentation and biochemical degradation, are still commonly used in many places to remove contaminants, such as pesticides, dyes, pharmaceutical waste and additional commercial waste products. Conventional water treatment typically includes several steps, such as the removal of suspended particles *via* macro-filtration in the initial phase of treatment and the oxidation of biological matter in the secondary phase of treatment. Next to secondary treatment, water may go through a tertiary treatment, which generally utilizes various kinds of chemicals, such as chlorine dioxide,[2] potassium permanganate,[3] chlorine[4] and ozone,[5] to carry out the process of chemical disinfection. UV radiation is also frequently utilized for this purpose.[6] After the final treatment step, water is usually micro-filtered and then discharged into the environment, where it can be utilized for *e.g.*, irrigation.[7]

[a]*Department of Chemistry, The Women University Multan, Kutchery Campus, Punjab, Pakistan. E-mail: drsara.chem@wum.edu.pk*

[b]*Pakistan Council of Research in Water Resources, Ministry of Water Resources, Pakistan*

[c]*Department of Zoology, College of Science, King Saud University, Riyadh 11451, Saudi Arabia*

[d]*Department of Botany and Microbiology, College of Science, King Saud University, Riyadh 11451, Saudi Arabia*

[e]*State Key Laboratory of Advanced Technology for Materials Synthesis and Processing, Wuhan University of Technology, Wuhan 430070, China*

[f]*National Research Tomsk Polytechnic University, Lenin Avenue 30, 634050 Tomsk, The Russian Federation*

To enhance the effectiveness of the treatment process, membrane technology has attracted significant attention due to its ability to ensure the efficient removal of contaminants, offering a promising solution for providing clean and uncontaminated water.[8] To achieve this objective, polymeric membranes are widely utilized for wastewater treatment and desalination. Organic membranes are generally preferred for separation purposes owing to their stability, adjustable hydrophobic and hydrophilic nature, potency for chemical reactions and remarkable mechanical strength.[9] Hence, there is great significance in utilizing polymers with the appropriate structural arrangement and adjustable chemical reactivity for the fabrication of separation membranes to aid purifying water. Among these, poly(paraphenylene terephthalamide), commonly known as aramid, is considered one of the strongest polymers.[10] Aramid has exceptional mechanical characteristics, a modifiable structure, dispersal ability, remarkable resistance against most commonly employed solvents, noteworthy thermal stability and physical and chemical endurance. These properties and the structural arrangement of aramid contribute towards its efficient membrane performance, even in challenging conditions. Consequently, aramid has found extensive application, including as a support in the fabrication of membranes for water purification.[11,12]

While membrane technology undoubtedly represents a versatile and efficient solution for water purification, offering a range of processes that can be tailored to meet specific water quality requirements in diverse applications, persistent biofouling can occur and poses a notable constraint hindering the optimal performance of the membrane. Addressing and mitigating the biofouling challenges is essential to unlock the full potential of membrane-based processes and ensure sustained efficiency in diverse industrial settings. To reduce this biofouling issue, various anti-biofouling agents, including organic, inorganic, and enzyme-dependent products, are frequently integrated into membranes, imparting antibacterial activity.[13]

In particular, inorganic anti-biofouling agents, such as silver,[14–17] graphene and graphene oxide,[18,19] gold,[20] copper,[21] CNTs,[22] TiO_2,[23] ZnO[24,25] and their nanocomposites,[26,27] have been investigated for integration into polymeric membranes to avoid biofouling due to bacteria. These biofouling agents can be used both in a nanosized form or immobilized onto supporting materials, such as CNTs,[28] graphene[29] and halloysite nanotubes,[30] to enhance their stability and longtime antibacterial ability.

The usage of organic modifiers as antifouling agents against bacteria can enhance the shelf-life of polymeric membranes.[13] Many researchers have used organic NPs in membranes to enhance the affinity of the organic modifiers with the polymers.[31,32] For instance, a prior study reported modifying the membrane through the integration of 2,4,6-triaminopyrimidine (TAP) and PVP, which could help prevent the loss of nanosized inorganic particles during long-term filtration processes.[33]

It was reported that 1,3-thiazolidine scaffolds exhibit remarkable antimicrobial properties and are potent against both bacteria and fungi. Moreover, they show antihypertensive and anti-inflammatory activities[34–36] and have potential against viruses too.[37] The range of their biological activities and potential is so diverse that researchers are actively engaged in exploring this platform for numerous biological activities.[36]

In the present study, a series of 2-substituted 1,3-thiazolidine-4-carboxylic acid nanoparticles (TNPs) were introduced as antifouling agents into aramid-based composite polypropylene (PP) membranes to reduce membrane fouling. For this purpose, various TNPs (**1a–5a**) were synthesized as antifouling agents. The structures of the precursor compounds are shown in Fig. 1. By incorporating TNPs, composite PP membranes were fabricated and are henceforth referred to as PP membranes (**PM-1** to **PM-5**). The synthesized TNPs were characterized by UV/Visible spectroscopy and XRD analyses, while the composite membranes loaded with the TNPs were characterized *via* SEM and FTIR analyses. Furthermore, the antibacterial properties of the synthesized TNPs and PP membranes loaded with the TNPs were evaluated against *E. coli*, while their antiviral properties were evaluated against the AIV-subtypes H9N2 and IBV as model strains.

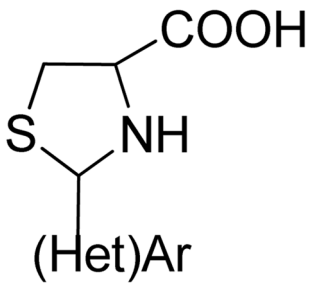

Fig. 1 Basic structure of the 2-phenyl-substituted 1,3-thiazolidine-4-carboxylic acid derivatives.

2 Experimental

2.1 Materials and method

All the chemicals used for synthesis of the TNPs and membranes were of analytical grade. Polypropylene, in pellet form with an isotactic structure and an average M_w of about 12 000, was obtained from Merck. Adipic acid, with a purity of 99.5%, was purchased from UNI-CHEM Chemical Reagents. Reagent grade *n*-hexane and isopropyl alcohol were obtained from Sigma-Aldrich. Sodium dodecyl sulfate (CAS-151-21-30) with high purity was provided by Merck. Soya-bean oil was purchased from a local market. UV/Visible analysis was performed by a double beam spectrophotometer (HALO DB-20). XRD analysis of the TNPs was carried out using an XRD spectrometer, namely the XPERT PRO XRD diffractometer (Panalytical, UK). The membranes were characterized by Fourier transform infrared (FTIR) spectroscopy using an ALPHA (PLATINIUM-ATR) FTIR spectrometer (range 375–4000 cm^{-1}). The morphology of the membranes was evaluated by SEM (JEOL 5410). A Zwick Roell-Z2.0 Universal Testing Machine, designed with a 2.5 kN Serie KS load cell and parallel jaw grips, was used for mechanical testing of the membrane samples.

2.2 Preparation of the 2-phenyl-substituted 1,3-thiazolidine-4-carboxylic acid derivatives (TNPs 1a–5a)

The TNPs (**1a–5a**) were synthesized using a solvent/antisolvent precipitation technique with the previously prepared 2-phenyl-substituted 1,3-thiazolidine-4-carboxylic acid derivatives (**1–5**),[38] with the structures of compounds **1–5** shown in Fig. 1. While, the structures of the aryl substituents in these compounds are illustrated in Table 1. For the synthesis of the TNPs, a solution was made by dissolving a compound (0.54 g) in 30 ml 2-propanol, and then distilled water (30 ml) was added to this solution to obtain a clear solution. The resulting solution was stirred at room temperature for 60 min and then left to stand for 1 day. Afterwards, the above-prepared solution was added to sodium dodecyl sulfate (SDS) solution (0.2% w/v), which had previously been prepared by dissolving SDS (0.2 g) in 100 ml distilled water to make the SDS solution. The resulting mixture was then centrifuged at 3500 rpm. The resulting precipitates were separated and washed with distilled water. The nanoparticles (NPs) were collected in a Petri dish and dried over 1 day at 60 °C [39] (Fig. 2a).

Fabrication of the nanosized 2-phenyl-1,3-thiazolidine-4-carboxylic acid was achieved by the following steps, which contributed to the development and stabilization of the nanoparticles. First, the compound was dissolved in a solvent to enable complete solubilization of the compound. The functional groups in the molecules, such as the carboxylic acid group and thiazolidine ring, were involved in the nucleation process, as they facilitate the intermolecular interactions necessary for nanoparticle development. Upon dissolving, the clear solution demonstrated that the compound was evenly dispersed. Afterwards, sodium dodecyl sulfate (SDS) was added as a surfactant in to the reaction system. SDS stabilized the nanoparticles, preventing their aggregation and reducing the surface tension, ensuring that the nanoparticles stayed separated and evenly dispersed throughout the medium. Finally, centrifugation at 3500 rpm facilitated the isolation of the nanoparticles from any by-products or other impurities in the solution. The nanoparticles of the 2-phenyl-1,3-thiazolidine-4-carboxylic acid derivatives were collected and characterized. The mechanism for the synthesis of the TNPs is shown in Fig. 2b.

In the structure of the 1,3-thiazolidine-4-carboxylic acid derivative the aryl group shows substitution.

2.3 Fabrication of TNP-functionalized aramid-supported PP membranes (PM-1 to PM-5)

The fabrication of **PM-1** to **PM-5** was carried out using a previously reported protocol.[40] First, PP polymer was heated in soybean oil at 300 °C, and then adipic acid was added with constant stirring (400 rpm) under heating until a homogenized solution was obtained. The TNPs were then sonicated in a dispersant (sodium polyacrylate) for 1 h at room temperature. After that, the TNP suspension was added to the polymer solution and stirred again to obtain a uniform phase. A piece of 4×7 cm^2 aramid fabric (as a support) was then inserted into the prepared solution and withdrawn instantly. Then, the membrane was dipped in distilled water for some time before being immersed in hexane for 12 h. The procedure to prepare the membranes is shown in Fig. 3.

Table 1 Structure of the aryl substituents in the 1,3-thiazolidine-4-carboxylic acid derivatives

Compounds	Het (Ar)	2-Phenyl-substituted 1,3-thiazolidine-4-carboxylic acids
1		2-Phenyl-1,3-thiazolidine-4-carboxylic acid
2	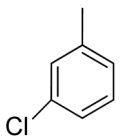	2-(3-Chlorophenyl)-1,3-thiazolidine-4-carboxylic acid
3	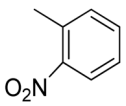	2-(2-Nitrophenyl)-1,3-thiazolidine-4-carboxylic acid
4	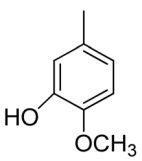	2-(3-Hydroxy-4-methoxyphenyl)-1,3-thiazolidine-4-carboxylic acid
5	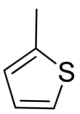	2-(2-Thienyl)-1,3-thiazolidine-4-carboxylic acid

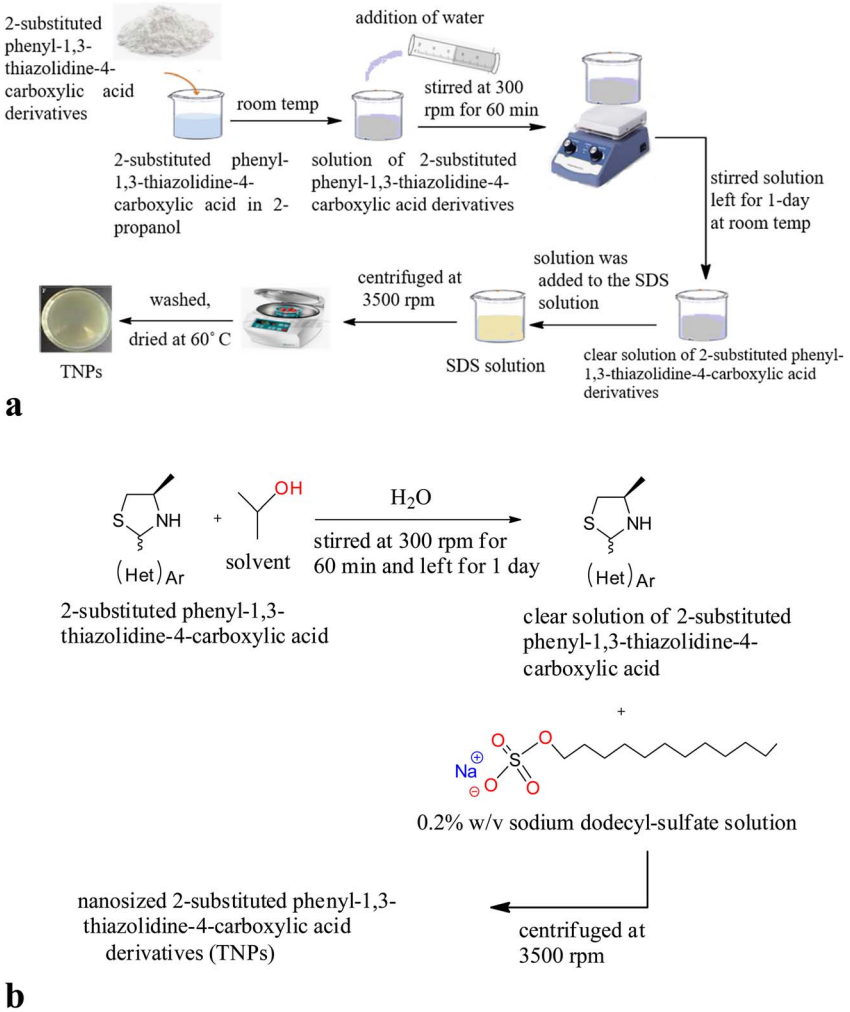

Fig. 2 (a) Preparation of nanoparticles of the 2-substituted phenyl-1,3-thiazolidine-4-carboxylic acid derivatives (TNPs **1a–5a**). (b) Reaction synthesis of the nanosized 2-substituted phenyl-1,3-thiazolidine-4-carboxylic acid derivatives (TNPs **1a–5a**).

2.4 Antibacterial bioassay

2.4.1 Strain preparation. For the antibacterial assay, the *E. coli* bacterial strain was obtained from Dr Imran Sajid, Department of MMG, Punjab University. A nutrient medium was used to keep the strain alive. For this assay, sterilized nutrient broth (50 ml) was taken in a conical flask (100 ml) and

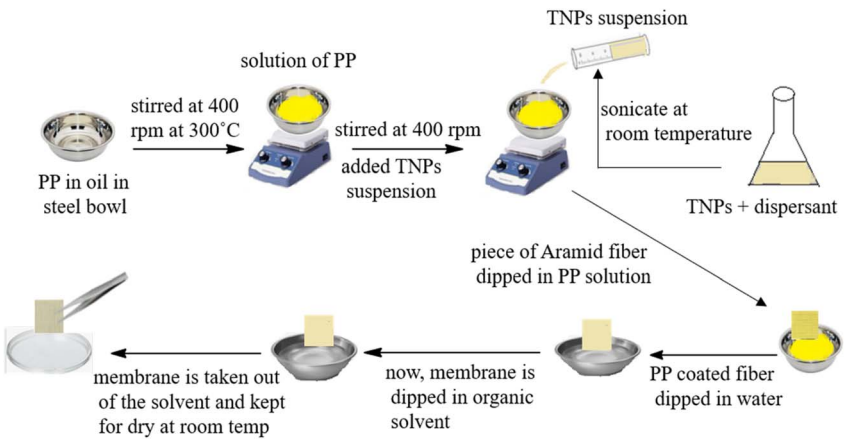

Fig. 3 Preparation of the aramid-based polymeric membranes (**PM-1** to **PM-5**).

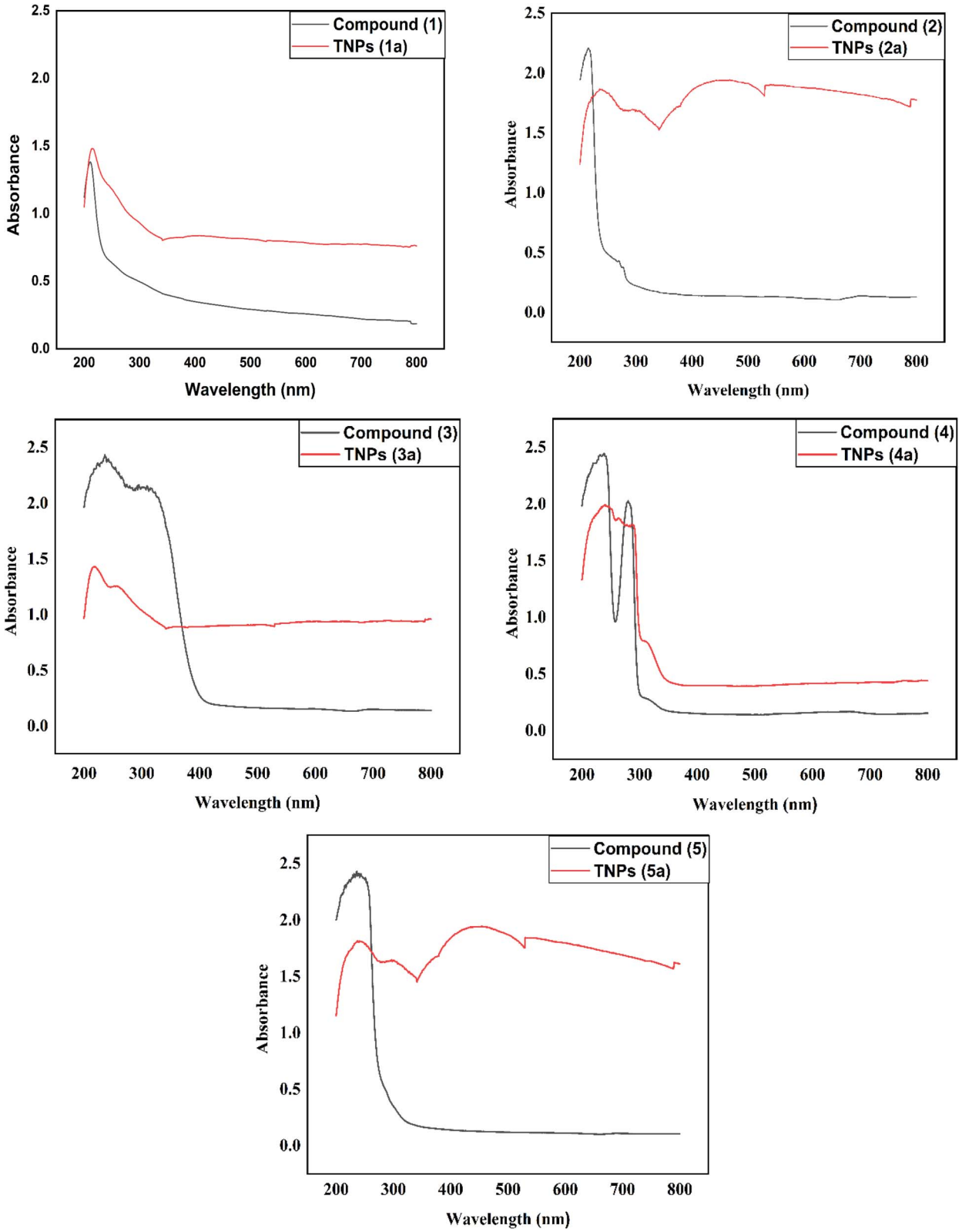

Fig. 4 UV-Visible spectra of the 2-phenyl-1,3-thiazolidine-4-carboxylic acid derivatives and their respective thiazolidine nanoparticles (TNPs).

used to transfer each bacterial strain (100 μl). After that, the bacterial strain was incubated for 24 h and cultured in the medium, *i.e.*, Muller–Hinton agar.[41]

2.4.2 Antibacterial assay. The antibacterial potentials of the TNPs and fabricated membranes were evaluated by the disk diffusion method. A disk or filter paper was coated with the test

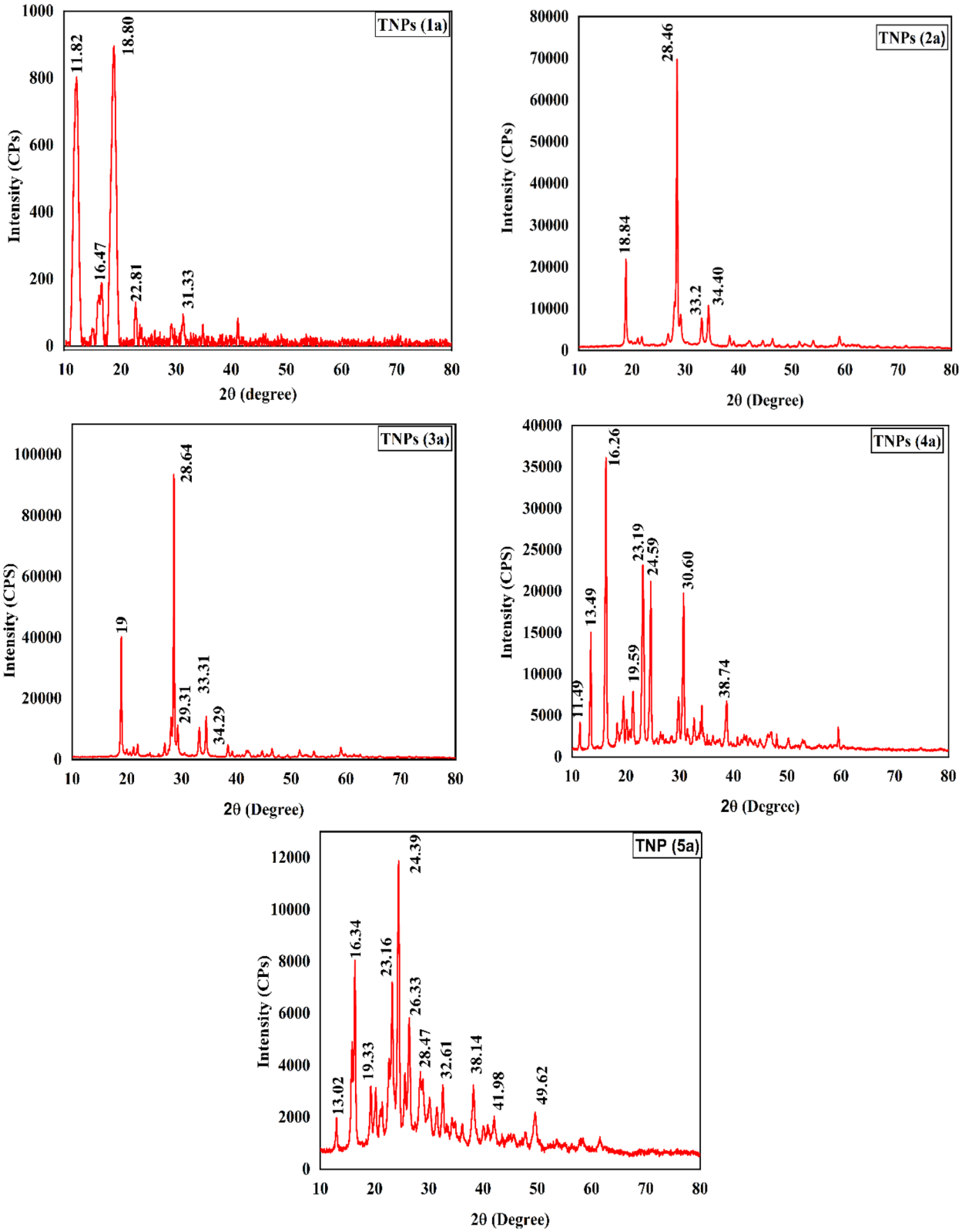

Fig. 5 XRD spectra of the nanoparticles of the 2-phenyl-1,3-thiazolidine-4-carboxylic acid derivatives (TNPs).

sample and was then placed on agar using an inoculation loop and then incubated overnight. After the incubation period, the plates were examined and the zones of inhibition were measured.[42] For testing the membrane, the Guango method[43] was followed, wherein the disc of the membrane, with the antibacterial agent, was placed on the agar surface with the bacterial strain. The disc was left for incubation overnight, and afterwards the zone of inhibition was measured.

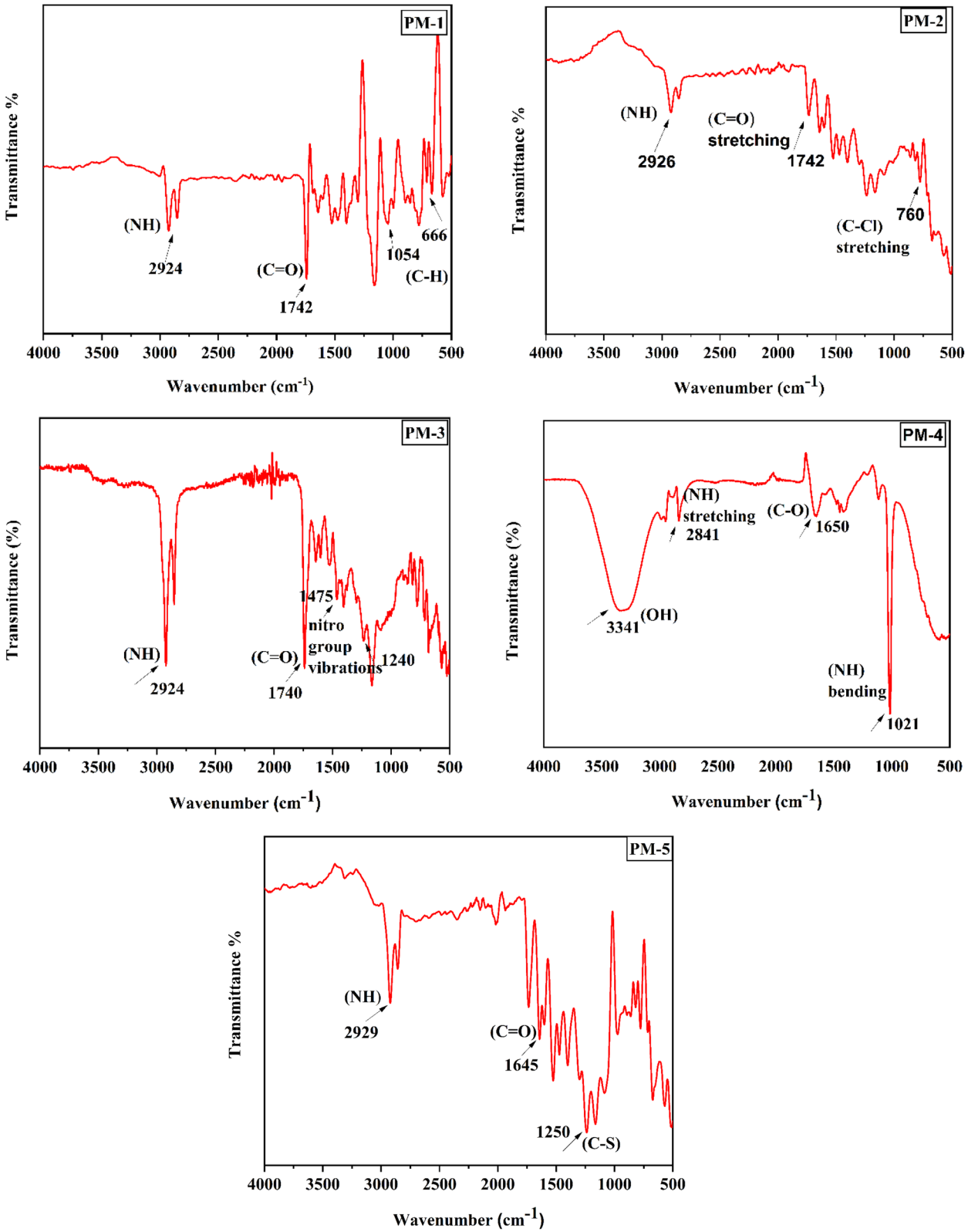

Fig. 6 IR spectra of the PP membranes (1–5) functionalized with the 2-(2-phenyl) 1,3-thiazolidine-4-carboxylic acid derivatives (TNPs).

2.4.3 Antiviral assay. The antiviral activities of the membranes (**PM-1** to **PM-5**) were evaluated against H9N2 and IBV viruses. For this, microbe-free chicken eggs were collected from the Govt. Poultry Farm, Bahawalpur, Pakistan. Meanwhile, the viral inoculants were received from the Department of Biochemistry and Molecular Biology Laboratory, University College of Veterinary and Animal Sciences, Islamia University, Bahawalpur, Pakistan. First, the viruses were inoculated in 9–11 day old chicken embryonated eggs by a chorioallantoic pathway,[44] with the whole procedure performed in biosafety cabinet II. Before inoculation, the eggs were candled, the wide area of the eggs was swabbed with ethanol (70%) and a hole was drilled in the eggs with an autoclaved pin. Strain was introduced into the eggs and the wider area was enclosed with molten wax. After that, the eggs were left to incubate at 37 °C for 72 h. Then, the allantoic fluids were collected and then subjected to testing by the hemagglutination (HA) test.[45]

2.4.4 *In ovo* antiviral assay. In order to evaluate the antiviral activities of the thiazolidines (**1–5**), the TNPs (**1a–5a**), and membranes (**PM-1** to **PM-5**), an *in ovo* antiviral assay was performed. For the thiazolidine derivatives and TNPs testing, an equal volume of thiazolidine and the viral suspension was injected into embryonated eggs and then incubated at 37 °C for 72 h. Afterward, allantoic fluid was collected for the HA test against H9N2 and IBV viruses.[46] Also, the same process was repeated for testing the NPs. To test the membranes, the same test method was used with some modifications. For this, same-sized pieces of membranes and an equal volume of viral suspension were injected into embryonated eggs and left for incubation at 37 °C. After 72 h, the fluid was tested for the HA virus.[47]

3 Results and discussion

3.1 Characterization of the prepared nanoparticles of 2-phenyl-1,3-thiazolidine-4-carboxylic acid derivatives (TNPs)

Confirmation of the prepared TNPs was performed by UV/Visible analysis, as shown in Fig. 4. The UV-Vis spectrum of the phenyl-substituted derivative (**1**) displayed a band at 210 nm, while the band for the respective TNPs (**1a**) was observed at 216 nm. The UV-Vis spectrum showed an absorption band for the chloro derivative of the standard thiazolidine 1,4 carboxylic acid (**2**) at 215 nm, while the band for the respective TNPs (**2a**) was observed at 230 nm. The UV-Vis spectrum of the nitro-substituted derivative (**3**) showed a band at 220 nm, while that of its nanoparticles (**3a**) appeared at 237 nm. The same pattern of bands was observed in the case of 2-(3-hydroxy-4-methoxyphenyl)-1,3-thiazolidine-4-carboxylic acid (**4**), where the compound showed a band at 236 nm, which was shifted to 247 nm during the fabrication of its nanoparticles (**4a**). The UV-Vis spectrum of 2-(2-thienyl)-1,3-thiazolidine-4-carboxylic acid displayed an absorption band at 231 nm, while that for its TNPs was observed at 249 nm.

The X-ray diffraction patterns of the TNPs are shown in Fig. 5. Different peaks were observed at various 2θ angles; *e.g.*, for TNPs (**1a**), peaks were observed at 11.82°, 16.47°, 18.80°,

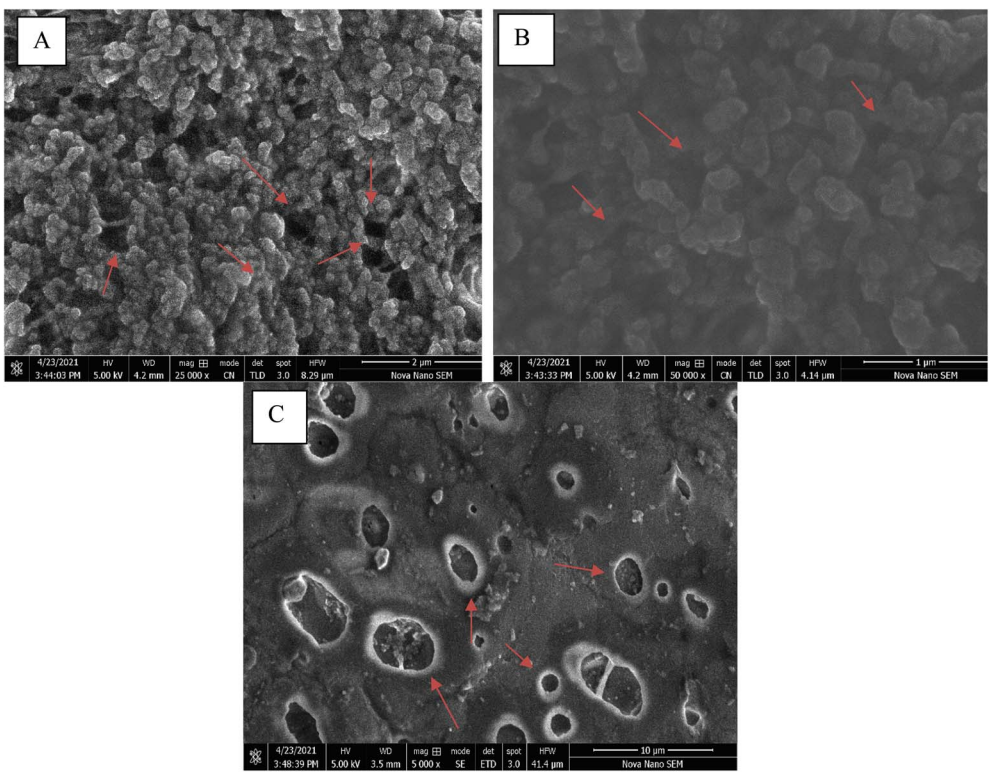

Fig. 7 Surface analysis of the PP membrane at 25 000× magnification (A), surface analysis of the PP membrane at 500 00× (B) with a working distance (WD) of 4.2 mm, and surface analysis of the PP membrane at 500 00× (C) with a working distance (WD) of 3.5 mm.

22.81°, 33.31°, while for TNPs (**2a**), peaks were observed at 18.84°, 28.46°, 33.20°, 34.40°. The nitro-derivative TNPs (**3a**) exhibited different peaks at 2θ angles of 19°, 28.64°, 33.31°, and 34.29°. Moreover, the hydroxy-4-methoxyphenyl derivative of TNPs (**4a**) and thienyl derivative of TNPs (**5a**) showed peaks at 2θ angles of 11.49°, 13.49°, 16.26°, 19.59°, 23.19°, 24.59°, 30.60°, 38.74° and 13.02°, 15.81°, 16.34°, 19.33°, 23.16°, 24.39°, 26.33°, 28.47°, 32.61°, 38.14°, 41.98°, respectively. The XRD patterns were also collected and used to determine the average particle sizes of the synthesized TNPs using the 2θ values and the Debye–Scherrer equation, as shown below.

$$D = K\lambda/B(\cos\theta)$$

Here, D shows the average size of the crystallites (nm), K is the crystallites shape constant (0.9), λ is the X-ray wavelength, B shows the full width at half maximum (FWHM) in radiation of the X-ray diffraction peak, and θ is Bragg's angle. The average particle sizes of the TNPs ranged from 28 to 30 nm.

3.2 Characterization of the fabricated aramid-supported PP membranes (PM-1 to PM-5)

The spectra of the various functional groups of the TNPs embedded in the polymeric membranes were observed in the range between 400–4000 cm^{-1} (Fig. 6). The spectrum of the phenyl-substituted TNPs embedded in the membrane (**PM-1**)

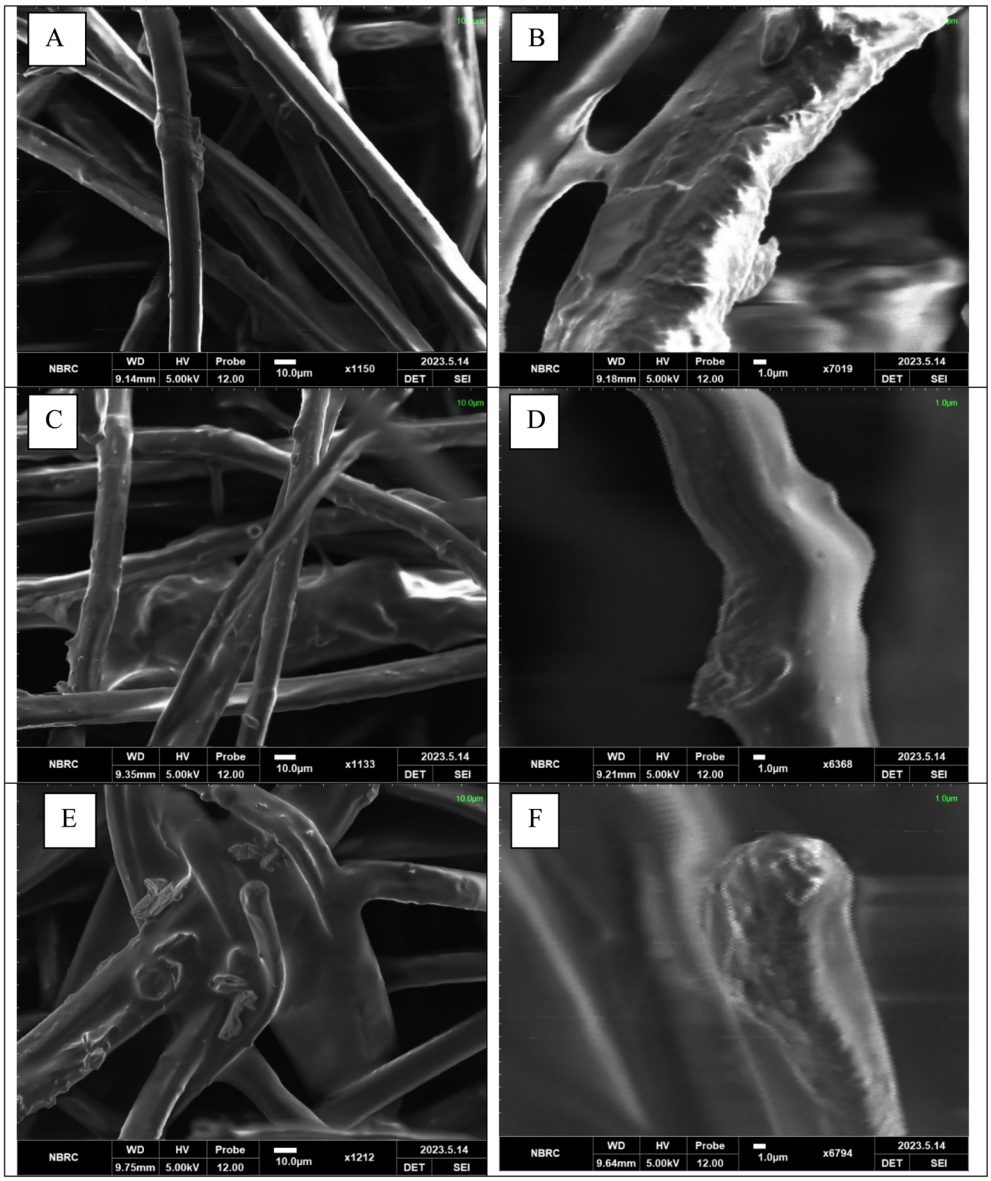

Fig. 8 A) Cross-sectional analysis of **PM-1** at 1150× magnification with a working distance (WD) of 9.14 mm. (B) Cross-sectional analysis of **PM-1** at 7019× magnification with a working distance (WD) of 9.18 mm. (C) Cross-sectional analysis of **PM-3** at 113× magnification with a working distance (WD) of 9.35 mm. (D) Cross-sectional analysis of **PM-3** at 6368× magnification with a working distance (WD) of 9.21 mm. (E) Cross-sectional analysis of **PM-5** at 1212× magnification with a working distance (WD) of 9.75 mm. (F) Cross-sectional analysis of **PM-5** at 6794× magnification with a working distance (WD) of 9.64 mm.

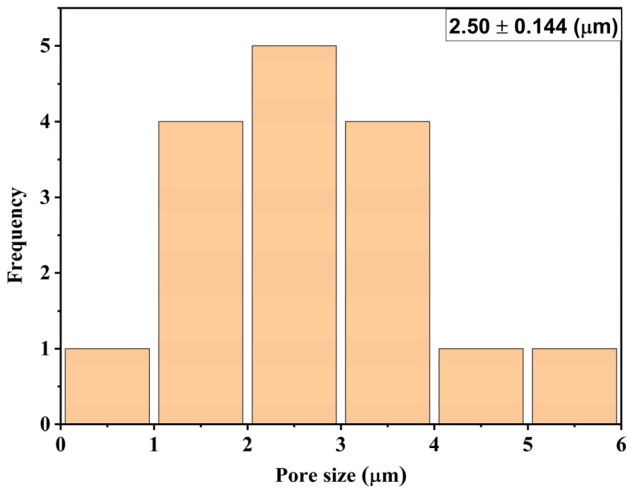

Fig. 9 Graphical representation of the pore sizes of the membranes.

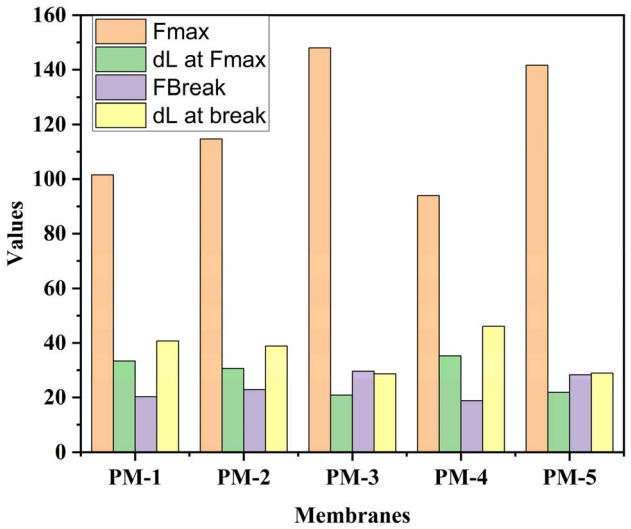

Fig. 10 Comparison of the mechanical properties of the membranes (PM-1 to PM-5).

exhibited –NH stretching at 2924 cm^{-1}, while a band for C=O appeared at 1742 cm^{-1}, and the phenyl showed C–H bending vibrations between 666–1054 cm^{-1}. The chloro derivative of the TNPs embedded in the membrane (**PM-2**) displayed a peak at 760 cm^{-1} associated with C–Cl stretching. Moreover, it exhibited –NH stretching at 2926 cm^{-1} and C=O stretching of a carboxylic acid group at 1742 cm^{-1}. Similarly, it was observed that the membrane (**PM-3**) functionalized with the TNPs of the nitro derivative showed several confirmation vibrations at 1240 and 1475 cm^{-1}, with these two peaks related to the nitro group. Moreover, –OH and –NH strong peaks were observed at 2924 cm^{-1} as well as C=O stretching at 1740 cm^{-1}. The 3-hydroxy-4-methoxy derivative of TNPs embedded in the membrane (**PM-4**) displayed –OH and –NH stretching bands at 3343 and 2841 cm^{-1} respectively. Besides, the C–O peak of the methyl phenyl ether and NH bending were observed at 1021 and 1650 cm^{-1}, respectively. Thus, the membrane (**PM-5**) functionalized with the thienyl derivative of TNPs displayed –NH stretching at 2929 cm^{-1} and a band for C=O that appeared at 1645 cm^{-1}.

In order to observe the surface characteristics of the membranes, they were subjected to SEM analysis. First, the PP membrane was examined under SEM, and images of it under different magnifications are shown in Fig. 7. The blank membrane was observed by SEM at 5.00 kV voltage with magnifications of 25 000× and 50 000×. At high magnification, the image of the PP membranes showed the presence of polymers hiding the aramid fiber, with some cavities depicted by red marks.

The cross-sectional characteristics of some of the polymeric membranes, *i.e.*, **PM-1**, **PM-3**, and **PM-5**, were examined by SEM analysis. SEM images of these membranes are shown in Fig. 8 and as captured with an electron voltage of 5 kV with different magnifications.

The pores in the membrane were the same size as those present in MF membranes; however, the hybrid membranes possessed three layers. The fabric middle layer was sandwiched between the top and bottom covers composed of a polymer, thus behaving as composite membranes. The membrane could filter in the NF range because of the crisscrossing pattern of the three layers. Similar results were documented in ref. 48. Generally, the pore size of composite membranes can range from nanometers to micrometers, based on the fabrication process and the intended function. Using SEM (Fig. 7C) and the ImageJ program, the pore sizes of these membranes were calculated and are shown in Fig. 9.

In order to evaluate the mechanical properties of the membranes, they were subjected to mechanical testing. The results showed that all the membranes were mechanically strong. Among all the membranes, **PM-3** demonstrated the highest F_{max} and F_{break}, showing that the PP membrane functionalized with the nitro-substituted compound had the ability to withstand pressure, indicating it was more resistant to rupturing. It also had the best mechanical strength. These findings show its strong structural integrity and high resistance to mechanical failure under stress. Other membranes *i.e.*, **PM-1** and **PM-2**, also showed good mechanical strength with some flexibility. **PM-4** demonstrated a moderate mechanical strength with low flexibility. **PM-5** had good mechanical resistance with moderate elongation. The mechanical properties of all these membranes are compared and shown in Fig. 10.

3.3 Evaluation of the disinfection ability

The 2-phenyl-substituted 1,3-thiazolidine-4-carboxylic acid derivatives (**1–5**), their respective nanoparticles (TNPs) (**1a–5a**) and the TNP-loaded aramid-based composite PP membranes (**PM-1** to **PM-5**) were evaluated against *E. coli* to assess their disinfection ability, and the results are shown in Table 2. Among the 2-substituted 1,3-thiazolidine-4-carboxylic acids (**1–5**), the nitro-substituted compound (**3**) proved to be more active, showing the maximum zone of inhibition; however, the TNPs prepared from these derivatives all showed good results compared to their bulk counterparts, which may be attributed to their small size distribution. The TNPs (**3a** and **5a**)-based

Table 2 Antibacterial activities of the 2-phenyl-substituted 1,3-thiazolidine-4-carboxylic acids (**1–5**), TNPs (**1a–5a**) and **PM-1** to **PM-5** membranes against *E. coli*[a]

Antimicrobial compounds (**1–5**)	Zone of inhibition (mm)	TNPs (**1a–5a**)	Zone of inhibition (mm)	Membranes	Zone of inhibition (mm)
1	08	**1a**	11	**PM-1**	09
2	09	**2a**	10	**PM-2**	07
3	11	**3a**	12	**PM-3**	10
4	08	**4a**	09	**PM-4**	06
5	10	**5a**	11	**PM-5**	10

[a] Ampicillin was used as a positive control (ZOI observed at 23 mm).

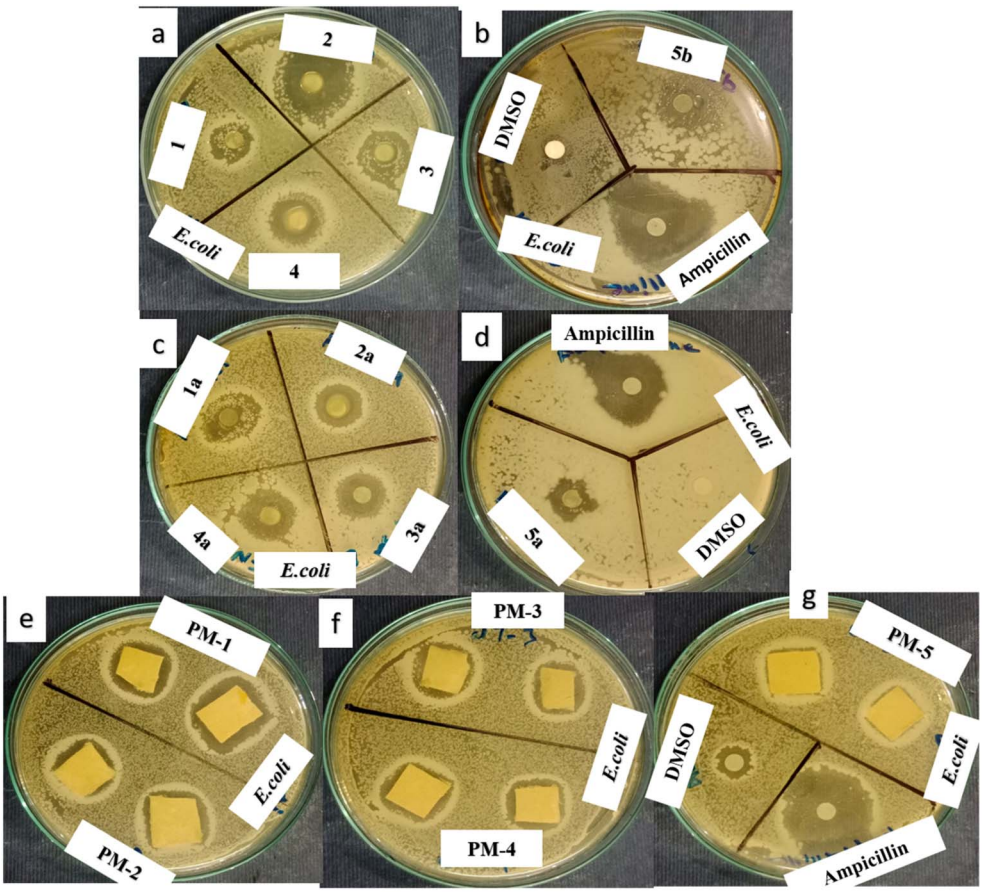

Fig. 11 Zone of inhibition against *E. coli* displayed by: (a and b) 2-phenyl-substituted 1,3-thiazolidine-4-carboxylic acids compounds (**1–5**), DMSO, and ampicillin (c and d), thiazolidine based nanoparticles, TNPs (**1a–5a**), DMSO, and ampicillin (e–g) polymeric membranes (**PM-1** to **PM-5**), DMSO, and ampicillin.

polymeric membranes (**PM-3** and **PM-5**) indicated excellent antifouling properties, and their zones of inhibition (ZOIs) are shown in Fig. 11.

All the synthesized materials were also evaluated for their antiviral activity and the results are shown in Table 3. As model viral strains, H9N2 and IBV were used for the antiviral evaluation. According to the data collected, the **PM-3** and **PM-5** membranes showed good antifouling properties. These membranes were considered to be good against H9. Also, these membranes proved to be more active against IBV. Images of the antiviral activity of the standard compounds, TNPs and membranes against AIV are shown in Fig. 12, while Fig. 13 shows the antiviral activity of the membranes against IBV.

The existing literature reveals a diverse range of polymers, such as PVDF, PES, and PSF, commonly enhanced with metallic nanoparticles, show varying degrees of efficacy against a spectrum of microbes, including *E. coli*. Based on the tabulated data above, it could be observed that the PP membranes enhanced with TNPs

Table 3 Antiviral activities of the 2-phenyl-substituted 1,3-thiazolidine-4-carboxylic acids (**1–5**), TNPs (**1a–5a**) and **PM-1** to **PM-5** membranes against AIV and IBV viruses

Standard compounds	AIV (H9N2) HA[a] (titre)	TNPs	AIV (H9N2) HA (titre)	Membranes	AIV (H9N2) HA (titre)	IBV HA (titre)
1	00	**1a**	08	**PM-1**	32	32
2	10	**2a**	02	**PM-2**	02	08
3	04	**3a**	00	**PM-3**	00	00
4	00	**4a**	02	**PM-4**	08	08
5	04	**5a**	00	**PM-5**	00	00
Normal saline (negative control)	1024					
DMSO (solvent control)	1024					
Amantadine (standard anti-AIV drug)	**2.70**					

[a] Hemagglutination (HA) titer 0–8: strongly effective drug (no growth or very limited growth of the virus); 16–32: effective drug (limited growth of the virus, the drug has controlled viral growth effectively); 64–128: moderately effective drug (the drug is not able to control the growth of the virus very efficiently, but it is still able to control the growth to some extent); 256–2048: ineffective drug (unable to control the growth of the virus).

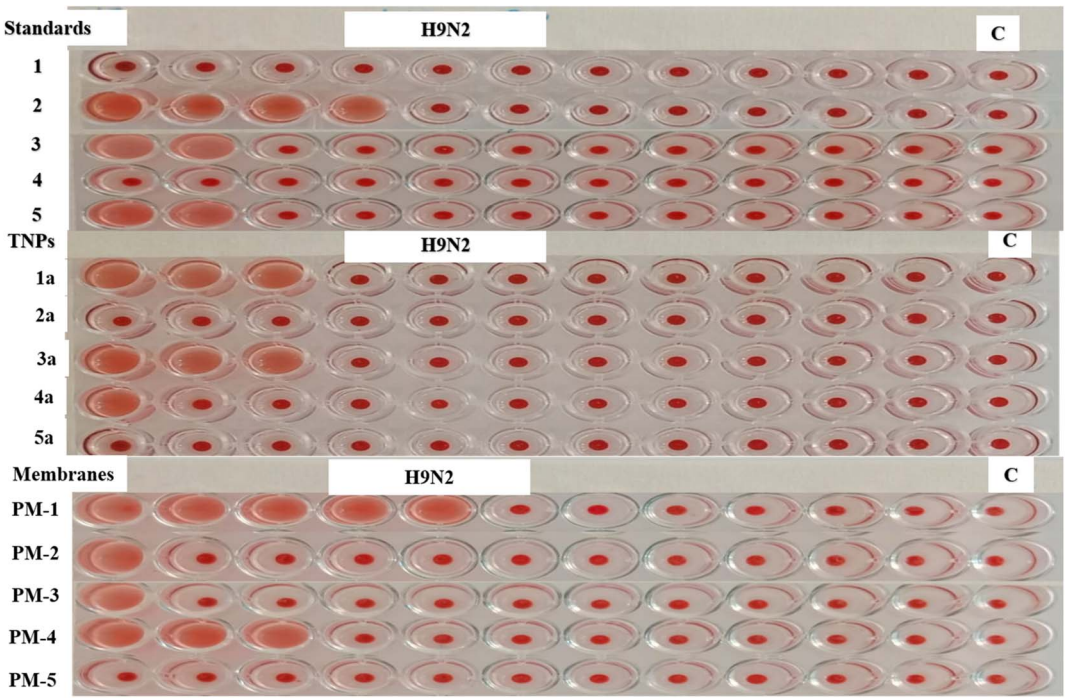

Fig. 12 Antiviral activities of the 2-phenyl-substituted 1,3-thiazolidine-4-carboxylic acids (**1–5**), TNPs (**1a–5a**) and **PM-1** to **PM-5** membranes against AIV.

fabricated in this study are superior to most previous reports as shown in Table 4. Notably, our study distinguishes itself in introducing a novel approach for enhancing antimicrobial properties targeting *E. coli*, H9N2 and IBV. This aspect presents a significant contribution to the field, addressing the limited antimicrobial effectiveness or the need for improved composite membranes.

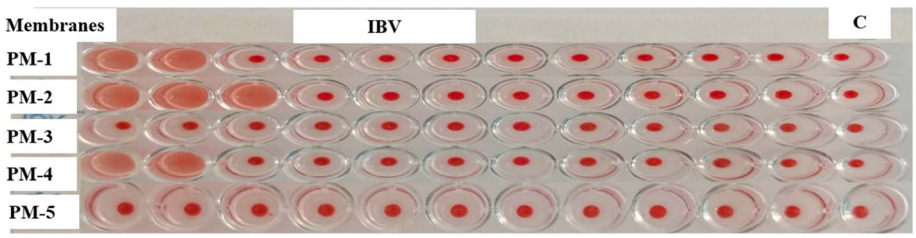

Fig. 13 Antiviral activity of the membranes (**PM-1** to **PM-5**) against IBV.

Table 4 Comparison of the various supported polymeric membranes targeting microbes[a]

Membranes	Fabrication technique	Porous/non-porous	Antimicrobial	Zone of inhibition (mm)	Reference
PES-PANCMA-PEI-Ag	Dry wet spinning process	Porous	Antibacterial	2.5–3	47
PAN/Ag-NPs	Electrospinning	Porous	*S. aureus* *E. coli*	8.45 ± 0.9	49
PSF/Cu_2O NPs	Phase inversion	Porous	*E. coli*	9.7 (±0.6)	50
PSF/ZnO	Phase inversion	Porous	*E. coli*	1.18	51
Aramid/PP/TNPs	Phase inversion	Porous	*E. coli*	10	Current study

[a] PES: polyether sulfone, PANCMA: poly acrylonitrile-*co*-maleic acid, PEI-Ag: polyethylene imine-silver, PAN: polyacrylonitrile, PSF: polysulfone, Cu_2O: cuprous oxide.

4 Conclusion

In this study, we successfully synthesized nanosized 2-phenyl-1,3-thiazolidine-4-carboxylic acids TNPs (**1a–5a**) utilizing a solvent/antisolvent precipitation technique. Furthermore, we developed polypropylene membranes (**PM-1** to **PM-5**) modified with these TNPs, demonstrating remarkable antifouling properties. Notably, all the synthesized TNPs exhibited significant antibacterial activity. Additionally, the TNP-based membranes, particularly those incorporated with nitro and thienyl TNPs, displayed significant antifouling efficacy against *E. coli*. In addition to their efficacy against *E. coli*, **PM-3** and **PM-5** demonstrated effectiveness against both IBV and the AIV subtype H9N2. Notably, owing to the increased surface area of the TNPs, they exhibited enhanced antiviral potency compared to their precursor compounds. Our study not only validates the existing research findings but also advances this field by unveiling insights into the enhanced antimicrobial efficacy achieved through the integration of TNPs into aramid-based polypropylene composite membranes.

5 Future perspectives

In the rapidly growing domain of water purification technology, the development of robust and high-performance membranes continues to be a primary focus. Aramid/PP composite membranes functionalized with nanosized 2-phenyl-1,3-thiazolidine-4-carboxylic acids have shown remarkable antimicrobial performance and the ability to reduce biofouling. Future research is anticipated to focus on boosting the longevity of these membranes, and expanding their antimicrobial scope to target a broader spectrum of pathogens, especially those involving multi-drug-resistant strains. Simultaneously, the exploration of environmentally benign materials is critical to ensure that these membranes do not harm the environment post-use when they may be discarded. A cost-effective fabrication method is also important in making these innovative membranes suitable for extensive use, particularly in water-treatment facilities at a large scale. Furthermore, real-world testing will continue to be essential for validating the membranes' effectiveness and compatibility with existing infrastructure, enabling their seamless implementation. Finally, the success of these advanced membranes will be measured by their impact on public health, particularly in areas facing water quality issues. This progress could mark a transformative era in membrane-based water-treatment technologies.

Data availability

The data that support the findings of this study are available from the corresponding author upon reasonable request.

Conflicts of interest

The authors declare no conflict of interest.

Acknowledgements

The authors acknowledge the Higher Education Commission of Pakistan's NRPU program (project #10312) and extend their sincere appreciation to the Researchers Supporting Project number (RSPD2025R694), King Saud University, Riyadh, Saudi Arabia.

References

1 R. P. Schwarzenbach, *et al.*, Global Water Pollution and Human Health, *Annu. Rev. Environ. Resour.*, 2010, **35**(1), 109–136, DOI: **10.1146/annurev-environ-100809-125342**.
2 E. M. Aieta, *et al.*, A review of chlorine dioxide in drinking water treatment, *J. – Am. Water Works Assoc.*, 1986, **78**(6), 62–72, DOI: **10.1002/j.1551-8833.1986.tb05766.x**.
3 A. K. Cherry, Use of potassium permanganate in water treatment, *J. – Am. Water Works Assoc.*, 1962, **54**(4), 417–424, DOI: **10.1002/j.1551-8833.1962.tb00862.x**.
4 H. Galal-Gorchev, Chlorine in water disinfection, *Pure Appl. Chem.*, 1996, **68**(9), 1731–1735, DOI: **10.1351/pac199668091731**.
5 W. H. Glaze, Drinking-water treatment with ozone, *Environ. Sci. Technol.*, 1987, **21**(3), 224–230, DOI: **10.1021/es00157a001**.
6 J. Sobotka, The efficiency of water treatment and disinfection by means of ultraviolet radiation, *Water Sci. Technol.*, 1993, **27**(3–4), 343–346, DOI: **10.2166/wst.1993.0372**.
7 M. Marcucci, *et al.*, Membrane Technologies Applied to Textile Wastewater Treatment, *Ann. N. Y. Acad. Sci.*, 2003, **984**(1), 53–64, DOI: **10.1111/j.1749-6632.2003.tb05992.x**.

8 K. Buruga, *et al.*, A review on functional polymer-clay based nanocomposite membranes for treatment of water, *J. Hazard. Mater.*, 2019, **379**, 120584, DOI: 10.1016/j.jhazmat.2019.04.067.

9 D. Rodríguez-San-Miguel, *et al.*, Processing of covalent organic frameworks: an ingredient for a material to succeed, *Chem. Soc. Rev.*, 2019, **48**(16), 4375–4386, DOI: 10.1039/C9CS00258H.

10 A. D. Roberts, *et al.*, Graphene–aramid nanocomposite fibres via superacid co-processing, *Chem. Commun.*, 2019, **55**(78), 11703–11706, DOI: 10.1039/C9CC04548A.

11 L. Liu, *et al.*, Multilayered membrane electrolytes based on aramid nanofibers for high-temperature proton exchange membrane fuel cells, *ACS Appl. Nano Mater.*, 2019, **2**(4), 2160–2168, DOI: 10.1021/acsanm.9b00144.

12 J. Lyu, *et al.*, Nanofibrous kevlar aerogel films and their phase-change composites for highly efficient infrared stealth, *ACS Nano*, 2019, **13**(2), 2236–2245, DOI: 10.1021/acsnano.8b08913.

13 J. Zhu, *et al.*, Polymeric antimicrobial membranes enabled by nanomaterials for water treatment, *J. Membr. Sci.*, 2018, **550**, 173–197, DOI: 10.1016/j.memsci.2017.12.071.

14 R. Manjumeena, *et al.*, Biogenic nanosilver incorporated reverse osmosis membrane for antibacterial and antifungal activities against selected pathogenic strains: an enhanced eco-friendly water disinfection approach, *J. Environ. Sci. Health, Part A*, 2014, **49**(10), 1125–1133, DOI: 10.1080/10934529.2014.897149.

15 S. Afkham, *et al.*, Fabrication of antimicrobial polyethersulfone microfiltration membranes by corona plasma-assisted coating of silver nanoparticles, *RSC Adv.*, 2016, **6**(109), 108113–108124, DOI: 10.1039/C6RA23257D.

16 L. F. Villalobos, *et al.*, In situ growth of biocidal AgCl crystals in the top layer of asymmetric polytriazole membranes, *RSC Adv.*, 2016, **6**(52), 46696–46701, DOI: 10.1039/C6RA08090A.

17 X. Zhao, *et al.*, Investigation of one-dimensional multi-functional zwitterionic Ag nanowires as a novel modifier for PVDF ultrafiltration membranes, *New J. Chem.*, 2016, **40**(1), 441–446, DOI: 10.1039/C5NJ02030A.

18 L. Karimi, *et al.*, Using graphene/TiO_2 nanocomposite as a new route for preparation of electroconductive, self-cleaning, antibacterial and antifungal cotton fabric without toxicity, *Cellulose*, 2014, **21**(5), 3813–3827, DOI: 10.1007/s10570-014-0385-1.

19 F. Perreault, *et al.*, Antimicrobial properties of graphene oxide nanosheets: why size matters, *ACS Nano*, 2015, **9**(7), 7226–7236, DOI: 10.1021/acsnano.5b02067.

20 K. Balasubramanian, Antibacterial application of polyvinylalcohol-nanogold composite membranes, *Colloids Surf., A*, 2014, **455**(1), 174–178, DOI: 10.1016/j.colsurfa.2014.04.050.

21 H.-Y. Wang, *et al.*, Synthesis of ultrastable copper sulfide nanoclusters via trapping the reaction intermediate: potential anticancer and antibacterial applications, *ACS Appl. Mater. Interfaces*, 2015, **7**(13), 7082–7092, DOI: 10.1021/acsami.5b01214.

22 C. Yang, *et al.*, Antimicrobial activity of single-walled carbon nanotubes: length effect, *Langmuir*, 2010, **26**(20), 16013–16019, DOI: 10.1021/la103110g.

23 X. Zhang, *et al.*, High-performance multifunctional TiO_2 nanowire ultrafiltration membrane with a hierarchical layer structure for water treatment, *Adv. Funct. Mater.*, 2009, **19**(23), 3731–3736, DOI: 10.1002/adfm.200901435.

24 S. T. Khan, *et al.*, ZnO and TiO_2 nanoparticles as novel antimicrobial agents for oral hygiene: a review, *J. Nanopart. Res.*, 2015, **17**(6), 1–16, DOI: 10.1007/s11051-015-3074-6.

25 S. Javdaneh, *et al.*, Engineering design of a biofilm formed on a pH-sensitive ZnO/PSf nanocomposite membrane with antibacterial properties, *RSC Adv.*, 2016, **6**(113), 112269–112281, DOI: 10.1039/C6RA11899B.

26 M. Arsalan, Fabrication, characterization, transportation of ions and antibacterial potential of polystyrene based $Cu_3(PO_4)_2$/$Ni_3(PO_4)_2$ composite membrane, *J. Ind. Eng. Chem.*, 2014, **20**(5), 3568–3577, DOI: 10.1016/j.jiec.2013.12.050.

27 S. Barua, *et al.*, One step preparation of a biocompatible, antimicrobial reduced graphene oxide–silver nanohybrid as a topical antimicrobial agent, *RSC Adv.*, 2014, **4**(19), 9777–9783, DOI: 10.1039/C3RA46835F.

28 V. K. Rangari, *et al.*, Synthesis of Ag/CNT hybrid nanoparticles and fabrication of their nylon-6 polymer nanocomposite fibers for antimicrobial applications, *Nanotechnology*, 2010, **21**(9), 095102, DOI: 10.1088/0957-4484/21/9/095102.

29 W. He, *et al.*, Photocatalytic and antibacterial properties of Au-TiO_2 nanocomposite on monolayer graphene: from experiment to theory, *J. Appl. Phys.*, 2013, **114**(20), 204701, DOI: 10.1063/1.4836875.

30 X. Ding, *et al.*, Preparation and antibacterial activity of copper nanoparticle/halloysite nanotube nanocomposites via reverse atom transfer radical polymerization, *RSC Adv.*, 2014, **4**(79), 41993–41996, DOI: 10.1039/C4RA03762F.

31 Y. Chen, *et al.*, Preparation and antibacterial property of polyethersulfone ultrafiltration hybrid membrane containing halloysite nanotubes loaded with copper ions, *Chem. Eng. J.*, 2012, **210**, 298–308, DOI: 10.1016/j.cej.2012.08.100.

32 I. Munnawar, *et al.*, Synergistic effect of Chitosan-Zinc Oxide Hybrid Nanoparticles on antibiofouling and water disinfection of mixed matrix polyethersulfone nanocomposite membranes, *Carbohydr. Polym.*, 2017, **175**, 661–670, DOI: 10.1016/j.carbpol.2017.08.036.

33 M. Ben-Sasson, *et al.*, Surface functionalization of thin-film composite membranes with copper nanoparticles for antimicrobial surface properties, *Environ. Sci. Technol.*, 2014, **48**(1), 384–393, DOI: 10.1021/es404232s.

34 Z.-C. Song, *et al.*, Synthesis, structure and structure–activity relationship analysis of 3-tert-butoxycarbonyl-2-arylthiazolidine-4-carboxylic acid derivatives as potential antibacterial agents, *Eur. J. Med. Chem.*, 2009, **44**(10), 3903–3908, DOI: 10.1016/j.ejmech.2009.04.014.

35 M. Mori, *et al.*, 2, 4-Dioxo-1, 3-thiazolidine derivatives as a lead for new fungicides, *J. Pestic. Sci.*, 2008, **33**(4), 357–363, DOI: **10.1584/jpestics.G08-15**.

36 M. OYA, *et al.*, Synthesis and antihypertensive activity of N-(mercaptoacyl)-thiazolidinecarboxylic acids, *Chem. Pharm. Bull.*, 1982, **30**(2), 440–461, DOI: **10.1248/cpb.30.440**.

37 N. Frimayanti, *et al.*, 2D, 3D-QSAR, and pharmacophore studies on thiazolidine-4-carboxylic acid derivatives as neuraminidase inhibitors in H3N2 influenza virus, *Med. Chem. Res.*, 2014, **23**(3), 1447–1453, DOI: **10.1007/s00044-013-0750-x**.

38 M. Mansouri, *et al.*, Preparation and characterization of ibuprofen nanoparticles by using solvent/antisolvent precipitation, *Open Conf. Proc. J.*, 2011, **2**(1), 88–94, DOI: **10.2174/2210289201102010088**.

39 S. Musaddiq, *et al.*, Thiazolidines: Potential anti-viral agents against avian influenza and infectious bronchitis viruses, *Vet. Res. Forum*, 2020, **11**(4), 415–421, DOI: **10.30466/vrf.2018.91264.2211**.

40 K. Mustafa, *et al.*, Fabrication of highly effective aramid fiber-based polypropylene composite membranes for desalination, *Korean J. Chem. Eng.*, 2023, **40**(11), 2735–2743, DOI: **10.1007/s11814-023-1534-8**.

41 M. Mama, *et al.*, Antibacterial Activity of Honey against Methicillin-Resistant Staphylococcus aureus. A Laboratory-Based Experimental Study, *Int. J. Microbiol.*, 2019, **2019**(1), 7686130–7686139, DOI: **10.1155/2019/7686130**.

42 G. Furtado, *et al.*, Single-disk diffusion testing (Kirby-Bauer) of susceptibility of Proteus mirabilis to chloramphenicol: significance of the intermediate category, *J. Clin. Microbiol.*, 1980, **12**(4), 550–553, DOI: **10.1128/jcm.12.4.550-553.1980**.

43 Y. Wu, *et al.*, Multiaction antibacterial nanofibrous membranes fabricated by electrospinning: an excellent system for antibacterial applications, *Nanotechnology*, 2009, **20**(24), 245101, DOI: **10.1088/0957-4484/20/24/245101**.

44 L. K. Sulaiman, *et al.*, In-ovo evaluation of the antiviral activity of methanolic root-bark extract of the African Baobab (Adansonia digitata Lin), *Afr. J. Biotechnol.*, 2011, **10**(20), 4256–4258, DOI: **10.5897/AJB10.2225**.

45 J.-X. Wang, *et al.*, An improved embryonated chicken egg model for the evaluation of antiviral drugs against influenza A virus, *J. Virol. Methods*, 2008, **153**(2), 218–222, DOI: **10.1016/j.jviromet.2008.06.022**.

46 K. C. Sekhar, *et al.*, Amino acid esters substituted phosphorylated emtricitabine and didanosine derivatives as antiviral and anticancer agents, *Appl. Biochem. Biotechnol.*, 2014, **173**, 1303–1318, DOI: **10.1007/s12010-014-0929-8**.

47 J. Prince, *et al.*, Self-cleaning Metal Organic Framework (MOF) based ultra filtration membranes-A solution to bio-fouling in membrane separation processes, *Sci. Rep.*, 2014, **4**(1), 6555, DOI: **10.1038/srep06555**.

48 C.-C. Wang, *et al.*, Hydrophilic and antibacterial properties of polyvinyl alcohol/4-vinylpyridine graft polymer modified polypropylene non-woven fabric membranes, *J. Membr. Sci.*, 2009, **345**(1–2), 223–232, DOI: **10.1016/j.memsci.2009.09.002**.

49 M. Sohrabi, *et al.*, Fabrication and evaluation of electrospun polyacrylonitrile/silver nanofiber membranes for air filtration and antibacterial activity, *Polym. Bull.*, 2023, **80**(5), 5481–5499, DOI: **10.1007/s00289-022-04311-1**.

50 Z. Xu, *et al.*, Preparation of Cu_2O nanowire-blended polysulfone ultrafiltration membrane with improved stability and antimicrobial activity, *J. Nanopart. Res.*, 2015, **17**, 1–9, DOI: **10.1007/s11051-015-3215-y**.

51 R. Rumintang, *et al.*, Synthesis and Characterization of Antibacterial ZnO - Functionalized Polysulfone Membrane, *Journal of Emerging Supply Chain, Clean Energy and Process Engineering*, 2022, **1**(1), 35–40, DOI: **10.57102/jescee.v1i1.14**.